

Multiple ambient hydrolysis deposition of tin oxide into nanoporous carbon as a stable anode for Lithium-ion batteries

The Faculty of Oregon State University has made this article openly available.
Please share how this access benefits you. Your story matters.

Citation	Raju, V., Wang, X., Luo, W. & Ji, X. (2014). Multiple Ambient Hydrolysis Deposition of Tin Oxide into Nanoporous Carbon To Give a Stable Anode for Lithium-Ion Batteries. Chemistry-A European Journal, 20(25), 7686-7691. doi:10.1002/chem.201402280
DOI	10.1002/chem.201402280
Publisher	John Wiley & Sons, Inc.
Version	Accepted Manuscript
Terms of Use	http://cdss.library.oregonstate.edu/sa-termsofuse

Energy storage

Multiple ambient hydrolysis deposition of tin oxide into nanoporous carbon as a stable anode for Lithium-ion batteries

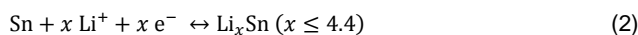
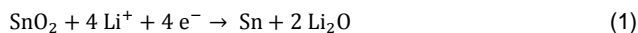
Vadivukarasi Raju, Xingfeng Wang, Wei Luo, Xiulei Ji*

Abstract: We introduce a novel ambient hydrolysis deposition (AHD) methodology that, for the first time, employs sequential water adsorption followed by a hydrolysis reaction to infiltrate tiny SnO₂ particles inside nanopores of mesoporous carbon in a conformal and controllable manner. The empty space in the SnO₂/C composites can be adjusted by varying the number of AHD cycles. A SnO₂/C composite with an intermediate SnO₂ loading exhibits an initial specific delithiation capacity of 1054 mAh/g as an anode for Li-ion batteries (LIBs). The capacity contribution from SnO₂ in the composite electrode

of SnO₂ (1494 mAh/g) when considering that both Sn alloying and SnO₂ conversion reactions are reversible. The composite shows a specific capacity of 573 mAh/g after 300 cycles, one of the most stable cycling performances for the SnO₂/mesoporous carbon composites. Enabled by the controllable AHD coatings, our results demonstrated the importance of the well-tuned empty space in nanostructured composites to accommodate the expansion of electrode active mass during alloying/dealloying and conversion reactions.

Introduction

Intense efforts have been devoted to exploring new electrode materials for Li-ion batteries (LIBs) in pursuing higher energy density and better cycling stability.^[1, 2] Compared to the conventional graphitic anodes, alloying anodes have attracted much attention due to their high theoretical capacities.^[3, 4] The primary challenge for alloying anodes is the very large volumetric changes during the Li alloying/dealloying processes, thus causing electrode pulverization and fast capacity fading.^[5, 6] Among the alloying anodes, SnO₂ is an attractive option due to its high theoretical capacity.^[7] During discharge, SnO₂ anodes operate via the following reactions:^[8]



The theoretical capacity is 782 mAh/g based on the assumption that only the alloying/dealloying reactions are reversible. The value is 1494 mAh/g if the conversion between Sn and SnO₂ is electrochemically reversible. The hurdle for SnO₂ as an anode has been its rapid capacity fading associated to the large Sn volume expansion (up to 259%) during Li⁺ insertion.^[9] To address this problem, one approach is to downsize the SnO₂ crystallites to minimize the strain during the alloying/dealloying reactions. Various SnO₂ nanostructures^[10, 11], such as nanotubes,^[12] nanosheets,^[13] hollow spheres,^[14] microboxes^[15] and mesoporous SnO₂^[16, 17] have been investigated. Studies on the correlation between the SnO₂ crystallite sizes and cycling stability revealed that SnO₂ nanoparticles of ~ 3 nm in diameter can exhibit a high capacity with improved cycling.^[18] However, maintaining a stable capacity for these single-component SnO₂ nanostructures has been very challenging.

Another approach is to encapsulate SnO₂ or Sn phases into a conducting conduit to accommodate the volumetric change.^[19, 20] An effective method is to homogeneously mix a tin precursor with organic carbon precursor(s) before a carbonization process. Yet, such synthetic route eliminates the possibility of using existing carbon materials that can be potentially desirable.^[21] As a result, efforts have been devoted to integrating SnO₂ or Sn into porous carbonaceous materials such as mesoporous carbon,^[22] porous graphene^[23, 24] and carbon nanotubes.^[25] To date, a number of infiltration methods, including sonochemical,^[26] chemical infiltration,^[27] wet-impregnation^[28] and sol-gel^[29] syntheses, electrostatic self assembly,^[30] have been investigated to incorporate active mass into nanoporous frameworks. Most recently, very promising results have been shown on

[a] Vadivukarasi Raju, Xingfeng Wang, Wei Luo, Xiulei Ji *
Department of Chemistry
Oregon State University
Corvallis
Oregon, U.S.A
* E-mail: david.ji@oregonstate.edu

Supporting information for this article is available on the WWW under <http://www.chemeurj.org/> or from the author.

SnO₂/graphene (or N-doped graphene) composites with very high capacities of over 1000 mAh/g and stable cycling.^[31,32] Despite the fact that excellent results have been achieved with different unique recipes,^[33] a general design principle for porous oxide/carbon composites has not been clearly demonstrated, to the best of our knowledge. This is due to the lack of precise synthetic control to manipulate the loading levels, morphology and dispersing uniformity of the encapsulated metal oxides in a carbon framework.

Herein, we utilize the ambient hydrolysis deposition (AHD) methodology developed in our laboratory for a layer-by-layer deposition of SnO₂ by pre-adsorbing water in a nanoporous carbon, CMK-3.^[34] Water adsorption in voids has been widely studied to understand the functions of water molecules in life activities of animals and plants.^[35,36] It is widely known that nanoporous materials, including nanoporous carbons, can adsorb water spontaneously at ambient conditions. This phenomenon has been investigated experimentally and by simulation work.^[37,38] We utilize this important phenomenon to help deposit controllable amounts of SnO₂ into a nanoporous carbon through a sequential water adsorption and hydrolysis reactions. We then investigated these tailor-designed materials as anodes for LIBs to address the volume-change challenge for SnO₂. A SnO₂/carbon composite with an intermediate loading of SnO₂ showed great cycling stability for 300 cycles with 573 mAh/g retained at a high current density 200 mA/g.

Results and Discussion

CMK-3, a long-range ordered mesoporous carbon was selected as the model carbon to study the layer-by-layer AHD for a deposition of SnO₂ as an anode material for LIBs. Briefly, AHD process involves a pretreatment of carbon with a mild oxidant, such as warm acidic ammonium persulfate (APS), to introduce hydrophilic groups on carbon surface. The obtained sample was designated as APS-CMK. Then, water was adsorbed into the carbon by equilibrating APS-CMK with saturated water vapor at 80 °C for one hour. Finally, the water-loaded sample was soaked in a non-aqueous solution of a tin precursor for one hour. The sample was then filtered in the glovebox. This sample was designated as 1-Sn-CMK. To increase SnO₂ loading, the sequential water-loading and hydrolysis process was repeated, and the samples were labeled as 2-Sn-CMK and 3-Sn-CMK.

Table 1. Physical characteristics of the samples

Sample	BET surface area (m ² /g)	Pore diameter (nm)	Pore volume (cm ³ /g)	SnO ₂ (wt%) (TGA)
CMK-3	1270	4.0	1.43	-
APS-CMK	1238	4.0	1.37	-
1-Sn-CMK	968	3.9	0.96	21
2-Sn-CMK	694	3.9	0.57	41
3-Sn-CMK	438	3.8	0.37	66

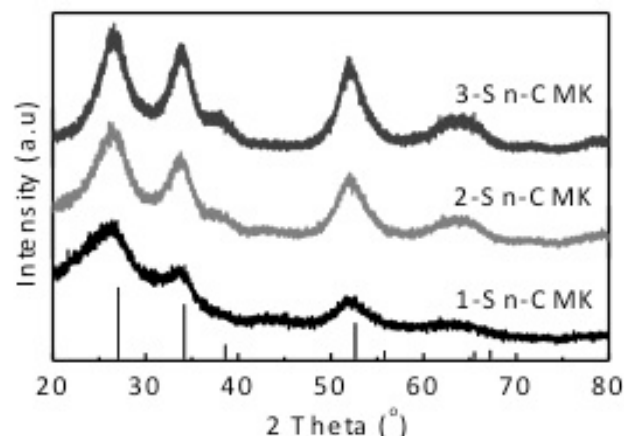


Figure 1. Wide angle XRD patterns of SnO₂/C composite after one, two and three cycles of AHD.

Figure 1 shows the X-ray diffraction patterns of samples prepared by first, second and third AHD cycle, respectively. These samples exhibited broad peaks at 25.7°, 33.2°, 36.9°, 50.8° and 62.3°, which can be indexed to (110), (101), (200), (211) and (301) planes of tetragonal SnO₂ (JCPDS 41-1445), respectively. These broad peaks suggest the existence of nanosized crystal domains of SnO₂. With increasing number of AHD cycles, the intensity of the XRD peaks increases, and the peaks turn slightly sharper, indicating a larger domain size of SnO₂ due to layer-by-layer growth. **Estimated by Scherrer Equation, the domain size increases from ~2 nm to ~5 nm from the first to the third AHD cycle with corresponding full width half maximum (FWHM) of XXX and XXX, respectively.** Table 1 summarizes the results from surface area and porosity measurements. The N₂ sorption isotherms and pore size distribution of the composites are presented in Figure 2a and Figure 2b, respectively. Treatment of CMK-3 with APS leads to a slight decrease in specific surface area and pore volume. As observed in the low-angle XRD patterns (supplementary Figure S1), the long-range order was well maintained. After one AHD cycle, the surface area and the pore volume decreased from 1238 m²/g and 1.37 cm³/g from the APS-CMK to 968 m²/g and 0.962 cm³/g, respectively. These parameters further decreased after the second and third AHD cycles.

The mass loading of the deposited SnO₂ in the composites was measured in air using thermogravimetric analysis (TGA) (Figure 2c). The small weight loss below 100 °C can be attributed to water evaporation. Almost no weight loss was observed between 100 °C and 400 °C, demonstrating the thermal stability of the composites in air up to 400 °C. The weight loss from 400 °C to 750 °C is due to carbon combustion. With increasing AHD cycles, the percentage of SnO₂ in the composites increases from 21 wt.% to 66 wt.%. When normalized for per gram of carbon, 0.26 g, 0.43 g and 1.30 g of SnO₂ was deposited after first, second and third AHD cycle. The dramatic increase of SnO₂ deposition in later AHD cycles can be attributed to the enhanced hydrophilic properties of the composite surface after the formation of SnO₂ layer.

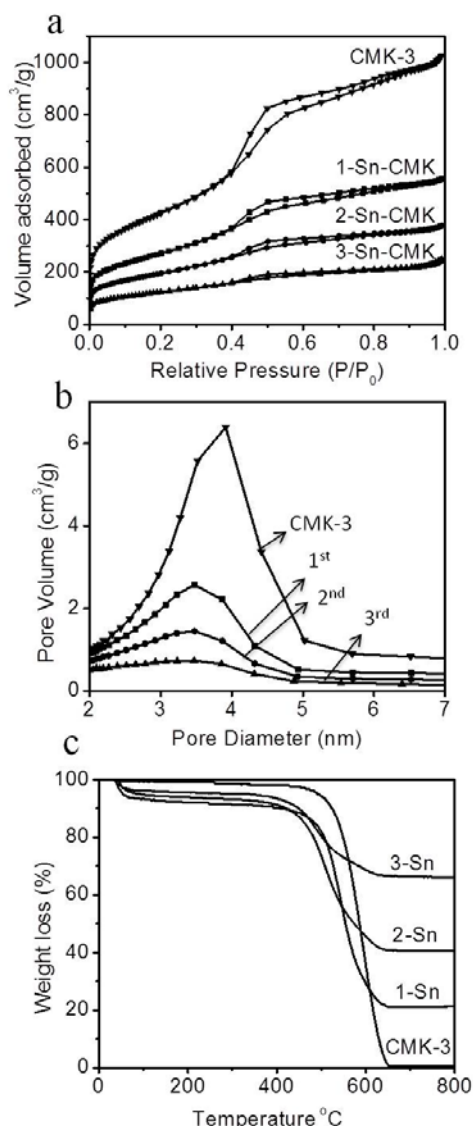


Figure 2. (a) N₂ adsorption-desorption isotherms of CMK-3, 1-Sn-CMK, 2-Sn-CMK and 3-Sn-CMK, (b) Pore size distribution profiles of pure CMK-3 and the composites after first, second and third AHD cycle, (c) TGA profiles of SnO₂/C composites after first, second and third AHD cycles.

To probe the morphology of the composites, scanning electron microscopy (SEM) and transmission electron microscope (TEM) studies were carried out on SnO₂/C composites (**Figure 3** and **Figure S2**). In the SEM images, the absence of SnO₂ nanoparticles indicates the successful loading of SnO₂ into the porous structure of CMK-3. (**Figure 3a** and **b**). From the TEM images, the fine dispersion of SnO₂ nanoparticles inside the channels of CMK-3 is evident (**Figure 3c**). HR-TEM analysis on 2-Sn-CMK shows the presence crystalline SnO₂ particles embedded in the carbon matrix (**Figure 3d** and **e**). **Figure 4** shows the high-angle angular dark field (HAADF) scanning TEM (HAADF-STEM) images and the corresponding carbon, oxygen and tin energy dispersive X-ray spectroscopy (EDX) mappings. Combining the information from HAADF-STEM and elemental mapping, it is clear that the SnO₂ nanoparticles in the composite

are of uniform particle size and are homogeneously dispersed within the mesoporous channels.^[39] EDX also indicated 43 wt.% SnO₂ in the composite, which corroborates the TGA measurements (**Figure S3**).

The electrochemical characteristics of the SnO₂/CMK composites were investigated in coin-style half-cells using lithium-metal foil as the counter electrode and 1.0 M LiPF₆ dissolved in ethylene carbonate and dimethyl carbonate (EC:DMC in the mass ratio of 1:1) as the electrolyte. Note that the specific capacity is calculated based on the total mass of a composite electrode. **Figure 5a** shows the first galvanostatic discharge/charge profiles of the SnO₂/CMK composites cycled

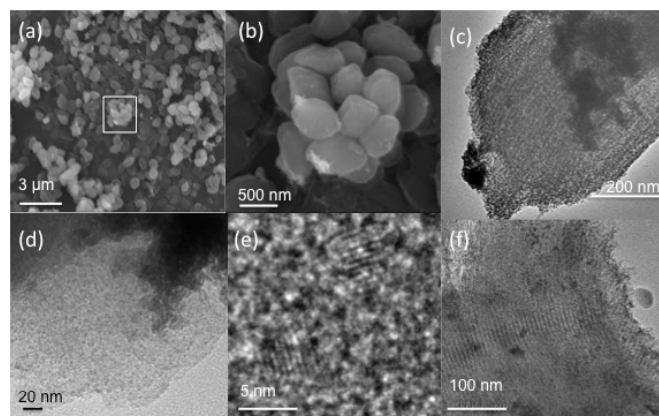


Figure 3. (a) SEM image of 2-Sn-CMK, (b) higher magnification image of the area inside the box in (a), (c) TEM image of 2-Sn-CMK (d) HR-TEM image of 2-Sn-CMK (e) HR-TEM image showing SnO₂ crystallites in 2-Sn-CMK (f) TEM image of 2-Sn-CMK after 300 galvanostatic cycles. Corresponding EDX mapping is shown in the Supporting Information.

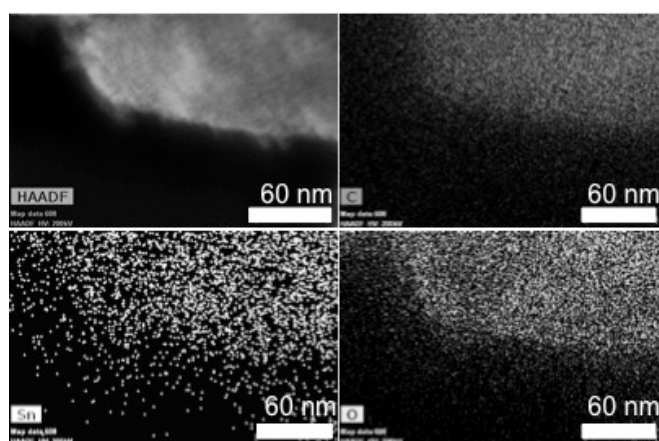


Figure 4. HAADF-STEM image for 2-Sn-CMK and the corresponding elemental mappings of carbon, tin and oxygen, respectively.

between 0.01 V to 2.0 V at a current density of 200 mA/g. For 2-Sn-CMK, the first discharge (lithiation) delivers a capacity of 2675 mAh/g, with a charge (delithiation) capacity of 1054 mAh/g,

exhibiting a 39% reversible capacity, while 1-Sn-CMK and 3-Sn-CMK have 33% and 46% reversible capacity, respectively. By comparing with the first discharge/charge profiles of APS-CMK with a 22% reversible capacity, one can see that a major portion of the irreversible capacity in the SnO₂/carbon composites is contributed from APS-CMK by forming a solid electrolyte interphase (SEI) layer (Supplementary information **Figure S4**).^[40] The reversibility, in fact, increases along higher SnO₂ loading. Certainly, SEI can be formed with the SnO₂ active mass as well, which contributes to the irreversible capacity.

The first delithiation capacity of 2-Sn-CMK, 1054 mAh/g, is much higher than 630 mAh/g for 1-Sn-CMK and 800 mAh/g for 3-Sn-CMK. It is generally accepted that only Li-Sn alloying process for SnO₂ electrodes is reversible, involving 4.4 Li⁺ per Sn atom, and the theoretical capacity of SnO₂ electrodes is 782 mAh/g. Based on the initial delithiation capacity of APS-CMK (603 mAh/g, **Figure S4**), the capacity contribution of SnO₂ in the first delithiation capacity of 2-Sn-CMK is 698 mAh/g_{composite}. The specific capacity for SnO₂ is calculated to be 1703 mAh/g that is even higher than the theoretical capacity of SnO₂ when 8.4 Li⁺ is reversibly inserted/deinserted (theoretical capacity of SnO₂: 1494 mAh/g). This surprising result may be due to the synergetic effect between porous carbon and SnO₂ nanoparticles, which might alter and enhance the electrochemical properties of the carbon matrix after SnO₂ deposition. The actual contribution from carbon may be underestimated in the composite. On the other hand, this result indicates that the conversion reaction of SnO₂ into Sn (Equation 1) in 2-Sn-CMK is reversible to a large extent. The actual cause for such a high specific capacity of SnO₂ is currently under investigating in our laboratories. It should be certain that the nanocrystalline nature of SnO₂ and the uniform dispersion of SnO₂ phases in a high surface area matrix would greatly enhance the electrochemical reactivity of SnO₂. Similar observations have been reported for ~ 2-6 nm SnO₂ nanoparticles embedded in graphene matrix, where the contribution from SnO₂ in the graphene composite reaches 94% of its theoretical capacity considering that both alloying and conversion reactions are reversible.^[41]

The first 50 charge/discharge cycles were tested at a current density of 200 mA/g for SnO₂/C composites after first, second and third AHD cycles, and the corresponding delithiation capacities are shown in **Figure 5b**. The composite of 2-Sn-CMK demonstrates a higher capacity of 684 mAh/g after 50 cycles. Surprisingly, 3-Sn-CMK shows a smaller capacity of 455 mAh/g and lower capacity retention (57%) after 50 cycles, compared to 2-Sn-CMK (65%). Here, we try to explain this phenomenon by a critical analysis based on the loading of SnO₂ and the available pore volume in the composites for Sn volume expansion. In 2-Sn-CMK, there is 0.695 g of SnO₂ per gram of carbon. According to Equation 1, SnO₂ undergoes a conversion reaction to form Sn and Li₂O, and Sn further alloys with Li⁺ to form Li_{4.4}Sn. Henceforth, it is possible to estimate the volume occupied by Li_{4.4}Sn and Li₂O, if we assume that nano-phases of Sn and Li₂O have the same density as their bulk counterparts. Thus, in 2-Sn-CMK, the SnO₂-derived mass would occupy a volume of 0.402 cm³/g_{carbon}, after the conversion and alloying reactions (assuming a 259 % volume expansion for Sn)^[9]. Considering that APS-CMK has a specific pore volume of 1.37 cm³/g, there would be sufficient pore volume in the 2-Sn-CMK at the end of lithiation for Sn. Similarly, in 3-Sn-CMK, SnO₂-derived mass, after complete conversion and

lithiation reactions, occupies a volume of 1.17 cm³/g_{carbon}. This expansion would fill up 85% of the available pore volume in the

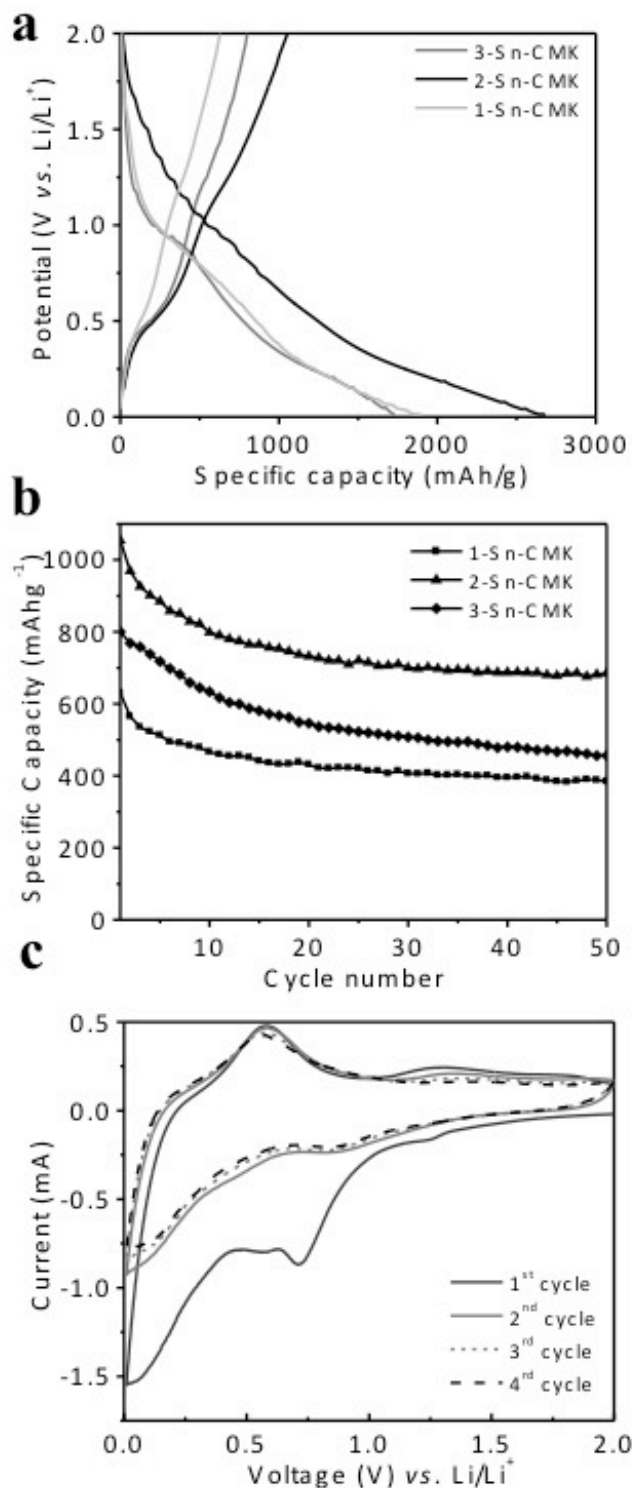


Figure 5. (a) The first-cycle galvanostatic discharge/charge profiles of SnO₂/CMK composites after the first, second and third AHD cycle at a current density of 200 mA/g, (b) Charge capacity cycling data for 1-Sn-CMK, 2-Sn-CMK and 3-Sn-CMK at a current density of 200 mA/g, (c) Cyclic voltammetry profiles of the initial four cycles of 2-Sn-CMK at a scan rate of 0.5 mV s⁻¹. Note that specific capacity is calculated based on the total weight of the composite.

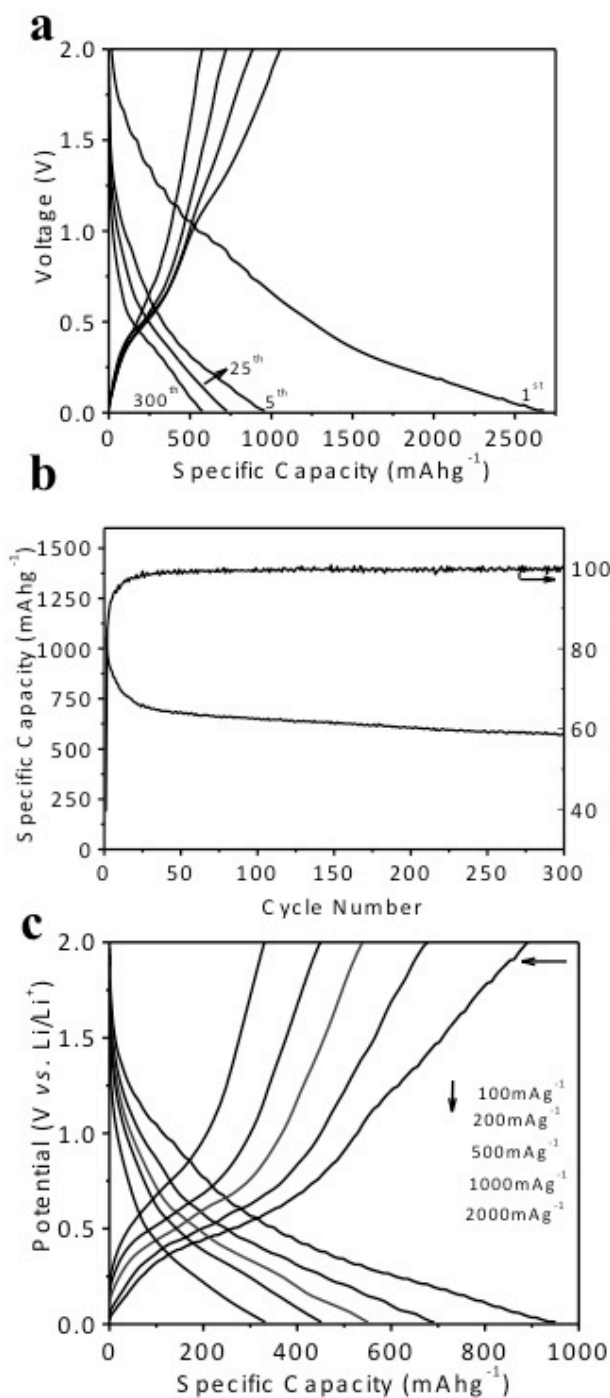


Figure 6. (a) Galvanostatic discharge/charge profiles of 2-Sn-CMK for the 1st, 5th, 25th and 300th cycle, (b) Long-term galvanostatic cycling performance and the corresponding Coulombic efficiency for 2-Sn-CMK at a current density of 200 mA/g, (c) Charge-discharge profiles of 2-Sn-CMK cycled at various current densities. Note that specific capacity is calculated based on the total weight of the composite.

APS-CMK, which may cause a serious strain for alloying and limits electrolyte imbibing. The large capacity difference from composites with different active mass loadings clearly shows the impact from the empty space in the composites on the electrochemical performance of the encapsulated SnO₂. Our results, for the first time, demonstrate the importance of porosity manipulation in nanoporous composites.

Due to its excellent performance, further electrochemistry investigations were carried out for the 2-Sn-CMK. **Figure 5c** shows the cyclic voltammetry (CV) measurements for 2-Sn-CMK at a scanning rate of 0.5 mV/s in the voltage window from 0.01 V to 2.0 V. In the cathodic scan, a large irreversible reduction peak was observed at 0.7 V, which is attributed to the decomposition of SnO₂ into Sn and Li₂O, and also to the formation of SEI on Sn phases and carbon. In the following CV cycles, a cathodic peak at 0.8 V still exists, indicative of a certain level of conversion reversibility of SnO₂.^[42] A pair of reversible redox peaks at 0.14 V and 0.55 V are assigned to the lithium alloying and dealloying with tin. These observations are in accordance with previous reports of SnO₂-based anodes.^[43,44] The largely unchanged peak current intensity, except for the first cycle, indicates good cycling stability of the composite electrode.

Long term galvanostatic cycling was conducted for 2-Sn-CMK between 0.01 V to 2.0 V at current density of 200 mA/g. The charge-discharge profiles of SnO₂/C composite at 1st, 5th, 25th and 300th cycles and the cycling profile are shown in **Figure 6a and 6b**. The coulombic efficiency increased from 85% in the second cycle to 99.6% in the 300th cycle. These results demonstrate the promising cycling stability for SnO₂ supported on mesoporous carbon and can be attributed to the well-managed microstructure of the composites. To further analyze the structural stability, TEM study was carried out on 2-Sn-CMK sample after 300 charge/discharge cycles (**Figure 3f**). From the TEM image, it is evident that mesoporous structure of CMK-3 was well maintained and there is no severe aggregation or agglomeration of SnO₂ particles. The corresponding HAADF scanning TEM image (HAADF-STEM) and EDX mapping of carbon, tin and oxygen reveals the uniform distribution of SnO₂ nanoparticles in the carbon matrix after 300 cycles (**Figure S5**). However, for 3-Sn-CMK after 200 cycles of charge-discharge, there is severe aggregation of SnO₂ particles (**Figure S6**). These results demonstrate the importance of a rigid three-dimensional carbon matrix for homogeneous dispersion of the SnO₂ nanoparticles and the manipulation of empty pore volume to accommodate the huge volume expansion/contraction of the tin nanoparticles during Li insertion/extraction process. Consequently in 2-Sn-CMK, the agglomeration of tin nanoparticles and the cracking or pulverization of electrode material upon prolonged cycling is alleviated, thus maintaining large capacity, high rate capability and cycling stability. Additionally, 3D porous architecture and the short diffusion channels enhance the Li-ion diffusion and accessible pathways to the surface of active materials. The

obtained specific capacity and the demonstrated number of cycles are higher than previous reports of similar composite with different preparation conditions (Supplementary information Table S1).^[45,26] For example, SnO₂ carbon composite hollow spheres exhibited a specific capacity of 473 mAh/g after 50 cycles.^[46] Another report for SnO₂ inside mesoporous carbon synthesized via a sonochemical method, showed a specific capacity of 200 mAh/g after 300 cycles.^[47] While using a melt injection method to form OMC-SnO₂ composites, a specific capacity of 472 mAh/g after 30 cycles was obtained.^[48]

Furthermore, the composite of 2-Sn-CMK exhibited excellent rate performance. The rate capability of SnO₂/C composite was investigated at different current rates of 100, 200, 500, 1000 and 2000 mA/g and the charge-discharge profiles are presented in **Figure 6c**. At a current rate of 2000 mA/g, a high capacity of 320 mAh/g was retained. This is higher than the reported rate performance of SnO₂-CNT,^[49] carbon coated SnO₂ platelets and SnO₂ embedded in mesoporous carbon.^[47] Moreover, even at high current densities high coulombic efficiency of 99% was maintained. The superior rate performance may be attributed to the large porosity within the composite and the conductive carbon framework.

Conclusion

We developed a new layer-by-layer AHD deposition methodology to conformably coat SnO₂ into a nanoporous carbon using sequential water adsorption and hydrolysis reactions. When investigated as anodes for LIBs, the composite with an intermediate loading exhibited stable a stable cycling performance with a capacity of 573 mAh/g retained after 300 cycles. This is superior to the SnO₂/mesoporous carbon composites previously reported. The enhancement is attributed to the fine manipulation of the empty pore volume in the porous composites to accommodate the volume expansion of Sn during alloying/dealloying reactions. We believe that the simple and scalable AHD methodology will potentially have a strong impact in many areas, including energy storage, separation and sensors.

Experimental Section

Materials and Preparation:

CMK-3 was prepared by a nanocasting method following the well-established procedure in the literature by employing SBA-15 as a hard template.

AHD method: Step I: Carbon surface functionalization. CMK-3 was treated with a mild oxidant, an acidic aqueous solution of (NH₄)₂S₂O₈, 1.0 M and H₂SO₄, 2 M. The carbon is referred to as APS-CMK. Typically, CMK-3, 0.3 g, was added to a freshly prepared 1.0 M APS acidic solution (30 ml). The mixture was stirred and refluxed at 60 °C for 6 hrs. Then, the solids were filtered, washed with deionized water and dried overnight in an oven at 80 °C.

Step II: Water loading. Degassed APS-CMK, 50 mg, was allowed to equilibrate in an ambient water vapor/air mixture with 100% relative pressure at 80 °C for one hour. Later, the sample was poured in to a Petridish and kept at stagnant atmosphere for one more hour.

Step III: Hydrolysis deposition of SnO₂. Water-loaded C-APS was dispersed and soaked for one hour in a dilute solution of Tin (IV) butoxide solvated in 1,3-dioxolane (DOXL) (10 vol%). The solid product was collected by filtration in a glovebox. Samples were heated at 300 °C under air for 5 hrs.

Characterization methods

X-Ray diffraction (XRD) patterns were collected using a Rigaku Ultima IV Diffractometer with Cu K α irradiation ($\lambda = 1.5406$ Å). The morphology was examined by field emission scanning electron microscopy (FESEM) using an FEI NOVA 230 high resolution SEM with an energy-dispersive X-ray (EDX) attachment. Transmission electron microscopy (TEM) images were recorded by FEI Titan 80-200 TEM. High-angle annular dark field scanning TEM (HAADF-STEM) measurements were carried out on an FEI Titan 80-200 microscope coupled with a HAADF detector and an EDX spectrometer. Nitrogen sorption measurements were performed on Micromeritics TriStar II 3020 analyzer. Thermogravimetric analysis (TGA) was performed using Shimadzu TGA-50 instrument under air from room temperature to 800 °C with a ramping rate of 10 °C min⁻¹.

Assembly and testing of Lithium-ion batteries

Slurries were prepared by mixing 80 wt% active material (SnO₂/C composite), 10 wt% carbon black (Super-P) and 10 wt% polyvinylidene fluoride (PVDF). The mixture was suspended in N-methyl-2-pyrrolidinone (NMP) before casting onto a Cu foil current collector by the doctor blade method. The typical active-mass loading is around 1-1.3 mg/cm². Lithium foil anodes were polished in an Ar environment before using as the counter/reference electrode. The electrodes were assembled in to a coin cell in the glovebox. Glass-fiber membrane was used as the separator, and 1 M LiPF₆ in ethylene carbonate (EC)/dimethyl carbonate (DMC) as the electrolyte. Galvanostatic cycling was conducted on an Arbin BT2000 system, and cyclic voltammograms (CVs) were collected on a VMP-3 multi-channel workstation at a scanning rate of 0.5 mVs⁻¹ at room temperature.

Acknowledgements

X. J. gratefully acknowledges the financial support from Oregon State University. We appreciate the help from Teresa Sawyer, and Dr. Peter Eschbach for their help in TEM measurements in OSU EM Facility that is funded by National Science Foundation, Murdock Charitable Trust and Oregon Nanoscience and Microtechnologies Institute. We are thankful to Dr. Douglas Keszler and Dr. Lev Zakharov for XRD measurements.

Keywords: Hydrolysis deposition • Lithium-ion batteries • Mesoporous materials • Sequential • SnO₂/C composite

- [1] M. Armand, J. M. Tarascon, *Nature* **2008**, *451*, 652-657.
- [2] X. Fang, B. Guo, Y. Shi, B. Li, C. Hua, C. Yao, Y. Zhang, Y. S.Hu, Z. Wang, G. D. Stucky, L. Chen, *Nanoscale* **2012**, *4*, 1541-1544.
- [3] C. M. Park, J. H. Kim, H. Kim, H. Sohn, *J. Chem. Soc. Rev.* **2010**, *39*, 3115-3141.
- [4] I. Kovalenko, B. Zdyrko, A. Magasinski, B. Hertzberg, Z. Milicev, R. Burtovyy, I. Luzinov, G. Yushin, *Science* **2011**, *334*, 75-79.
- [5] H. Liu, X. Du, X. Xing, G. Wang, S. Z. Qiao, *Chem. Commun.* **2012**, *48*, 865-867.
- [6] H. Liu, D. Su, R. Zhou, B. Sun, G. Wang, S. Z. Qiao, *Adv. Energy Mater.* **2012**, *2*, 970-975.

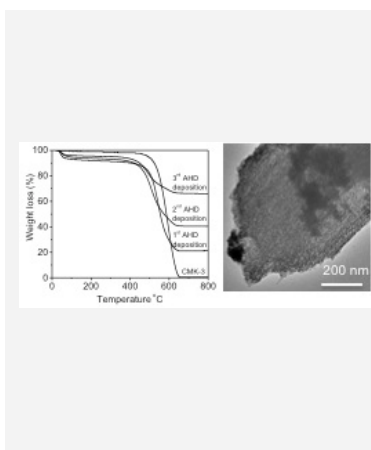
- [7] J. S. Chen, X. W. Lou, *Small* **2013**, *9*, 1877-1893.
- [8] J. Y. Huang, L. Zhong, C. M. Wang, J. P. Sullivan, W. Xu, L. Q. Zhang, S. X. Mao, N. S. Hudak, X. H. Liu, A. Subramanian, H. Fan, L. Qi, A. Kushima, J. Li, *Science* **2010**, *330*, 1515-1520.
- [9] I. A. Courtney, J. R. Dahn, *J. Electrochem. Soc.* **1997**, *144*, 2045-2052.
- [10] Z. Wang, Z. Wang, S. Madhavi, X. W. Lou, *J. Mater. Chem.* **2012**, *22*, 2526-2531.
- [11] S. Ding, Z. Wang, S. Madhavi, X. W. Lou, *J. Mater. Chem.* **2011**, *21*, 13860-13864.
- [12] J. Ye, H. Zhang, R. Yang, X. Li, L. Qi, *Small* **2010**, *6*, 296-306.
- [13] C. Wang, G. Du, K. Stahl, H. Huang, Y. Zhong, J. Z. Jiang, *J. Phys. Chem. C* **2012**, *116*, 4000-4011.
- [14] S. Ding, X. W. Lou, *Nanoscale* **2011**, *3*, 3586-3588.
- [15] L. Zhang, H. B. Wu, B. Liu, X. W. Lou, *Energy Environ. Sci.* **2014**, *7*, 1013-1017.
- [16] R. Demir-Cakan, Y.-S. Hu, M. Antonietti, J. Maier, M. M. Tititici, *Chem. Mater.* **2008**, *20*, 1227-1229.
- [17] H. Liu, S. Chen, G. Wang, S. Z. Qiao, *Chem. Euro. J.* **2013**, *19*, 16897-16901.
- [18] C. Kim, M. Noh, M. Choi, J. Cho, B. Park, *Chem. Mater.* **2005**, *17*, 3297-3301.
- [19] J. Hassoun, G. Derrien, S. Panero, B. Scrosatti, *Adv. Mater.* **2008**, *20*, 3169-3175.
- [20] S. Xin, Y.-G. Guo, L.-J. Wan, *Acc. Chem. Res.* **2012**, *45*, 1759-1769.
- [21] Y. Xu, Q. Liu, Y. Zhu, Y. Liu, A. Langrock, M. R. Zachariah, C. Wang, *Nano Lett.* **2013**, *13* (2), 470-474.
- [22] J. Fan, T. Wang, C. Z. Yu, B. Tu, Z. Y. Jiang, D. Y. Zhao, *Adv. Mater.* **2004**, *16*, 1432-1436.
- [23] S. M. Paek, E. Yoo, I. Honma, *Nano Lett.* **2009**, *9*, 72-75.
- [24] X. J. Zhu, Y. W. Zhu, S. Murali, M. D. Stoller, R. S. Ruoff, *J. Power Sources* **2011**, *196*, 6473-6477.
- [25] H. Zhang, H. Song, X. Chen, J. Zhou, H. Zhang, *Electrochimica Acta* **2012**, *59*, 160-167.
- [26] H. Qiao, J. Li, J. Fu, D. Kumar, Q. Wei, Y. Cai, F. Huang, *ACS Appl. Mater. Interfaces* **2011**, *3*, 3704-3708.
- [27] J. Chen, K. Yano, *ACS Appl. Mater. Interfaces* **2013**, *5*, 7682-7687.
- [28] F. M. Hassan, Z. Chen, A. Yu, Z. Chen, X. Xiao, *Electrochimica Acta* **2013**, *87*, 844-852.
- [29] S. Xu, Y. Hong, C. Chen, S. Li, L. Xiao, J. Fan, *J. Mater. Chem. A* **2013**, *1*, 6191-6198.
- [30] X. Zhou, Y.-X. Yin, L.-J. Wan, Y.-G. Guo, *Adv. Energy Mater.* **2012**, *2*, 1086-1090.
- [31] X. Zhou, L.-J. Wan, Y.-G. Guo, *Adv. Mater.* **2013**, *25*, 2152-2157.
- [32] L.-S. Zhang, L.-Y. Jiang, H.-J. Yan, W. D. Wang, W. Wang, W.-G. Song, Y.-G. Guo, L.-J. Wan, *J. Mater. Chem.* **2010**, *20*, 5462-5467.
- [33] Y. Xu, Q. Liu, Y. Zhu, Y. Liu, A. Langrock, M. R. Zachariah, C. Wang, *Nano Lett.* **2013**, *13* (2), 470-474.
- [34] X. Wang, V. Raju, W. Luo, B. Wang, W. F. Stickle, X. Ji, *J. Mater. Chem. A* **2014**, *2*, 2901-2905.
- [35] T. Ohba, H. Kanoh, K. Kaneko, *J. Am. Chem. Soc.* **2004**, *126*, 1560-1562.
- [36] T. Ohba, H. Kanoh, K. Kaneko, *Chem. Eur. J.* **2005**, *11*, 4890-4894.
- [37] A. Striolo, A. A. Chialvo, P. T. Cummings, K. E. Gubbins, *Langmuir* **2003**, *19*, 8583-8591.
- [38] M. Bellissent-Funel, R. Sridi-Dorbez, L. Bosio, *J. Chem. Phys.* **1996**, *104*, 10023-10029.
- [39] X. Pan, X. Bao, *Chem. Comm.* **2008**, 6271.
- [40] J. C. Arrebola, A. Caballero, L. Hernan, J. Morales, *J. Electrochem. Soc.* **2009**, *156*, A986-A992.
- [41] P. C. Lian, X. F. Zhu, S. Z. Liang, Z. Li, W. S. Yang, H. H. Wang, *Electrochim. Acta* **2011**, *56*, 4532-4539.
- [42] X. W. Lou, Y. Wang, C. Yuan, J. Y. Lee, L. A. Archer, *Adv. Mater.* **2006**, *18*, 2325-2329.
- [43] N. C. Li, C. R. Martin, *J. Electrochem. Soc.* **2001**, *148*, A164-A170.
- [44] L. Zhang, G. Zhang, H. B. Wu, L. Yu, X. W. Lou, *Adv. Mater.* **2013**, *25*, 2589-2593.
- [45] F. Han, W.-C. Li, M.-R. Li, A.-H. Lu, *J. Mater. Chem.* **2012**, *22*, 9645-9651.
- [46] X. W. Lou, D. Deng, J. Y. Lee, L. A. Archer, *Chem. Mater.* **2008**, *20*, 6562-6566.
- [47] Z. Yu, S. Zhu, Y. Li, Q. Liu, C. Feng, D. Zhang, *Mater. Lett.* **2011**, *65*, 3072-3075.
- [48] C. Lin, Y. Hu, F. Jiang, G. Chen, *Mater. Lett.* **2013**, *94*, 83-85.
- [49] X. Liu, M. Wu, M. Li, X. Pan, J. Chen, X. Bao, *J. Mater. Chem. A* **2013**, *1*, 9527-9535.

Energy Storage

Vadivukarasi Raju, Xingfeng
Wang, Wei Lou, Xiulei Ji*

..... Page – Page

**Layer-by-layer ambient
hydrolysis deposition of tin oxide
into nanoporous carbon as a
stable anode for Lithium-ion
batteries**



Novel ambient hydrolysis deposition methodology employs sequential water adsorption and hydrolysis to form tiny SnO₂ nanoparticles inside nanoporous carbon. The SnO₂/C composite materials exhibit superior performance and enhanced cycling stability as anode materials for Lithium-ion batteries.